Transcription 3:5, 260-269; September/October 2012; © 2012 Landes Bioscience

RNA polymerase stalls in a post-translocated register and can hyper-translocate

Yuri A. Nedialkov,[1,2] Evgeny Nudler[2] and Zachary F. Burton[1,*]

[1]Department of Biochemistry and Molecular Biology; Michigan State University; East Lansing, MI USA; [2]Department of Biochemistry; New York University Medical Center; New York, NY USA

Keywords: RNA polymerase, bridge helix, trigger loop, tagetitoxin, translocation, hyper-translocation, NTP analogues

Abbreviations: *E. coli*, *Escherichia coli*; Exo III, exonuclease III; GMPcPP, α,β-methylene guanosine triphosphate; NTP, nucleoside triphosphate; nt, nucleotide; PPi, pyrophosphate (diphosphate); RNAP, RNA polymerase; RNA-G9, 9 nucleotide RNA ending in 3'-GMP; TEC, ternary elongation complex (RNAP, DNA, nascent RNA)

Exonuclease (Exo) III was used to probe translocation states of RNA polymerase (RNAP) ternary elongation complexes (TECs). *Escherichia coli* RNAP stalls primarily in a post-translocation register that makes relatively slow excursions to a hyper-translocated state or to a pre-translocated state. Tagetitoxin (TGT) strongly inhibits hyper-translocation and inhibits backtracking, so, as indicated by Exo III mapping, TGT appears to stabilize both the pre- and probably a partially post-translocation state of RNAP. Because the pre-translocated to post-translocated transition is slow at many template positions, these studies appear inconsistent with a model in which RNAP makes frequent and rapid (i.e., millisecond phase) oscillations between pre- and post-translocation states. Nine nucleotides (9-nt) and 10-nt TECs, and TECs with longer nascent RNAs, have distinct translocation properties consistent with a 9–10 nt RNA/DNA hybrid. RNAP mutant proteins in the bridge helix and trigger loop are identified that inhibit or stimulate forward and backward translocation.

Introduction

How RNA polymerase (RNAP) ternary elongation complexes (TECs) move between template translocation positions continues to be controversial.[1-10] Although some crystal structures of TECs can be pre-translocated,[11,12] a post-translocated register is more often observed indicating that RNAP may rest in a primarily post-translocated state.[12-16] Using a fluorescence assay for translocation, *Escherichia coli* (*E. coli*) RNAP was found to rest in a predominantly post-translocated register, and the antibiotic tagetitoxin (TGT) held RNAP in a more pre-translocated position.[10] TGT was hypothesized to mimic pyrophosphate to stabilize the pre-translocated TEC and to limit downstream excursions by RNAP.[10,17-19] Using an innovative α-hemolysin nanopore single elongation complex procedure, Phi29 DNA polymerase (DNAP), which is not homologous to multi-subunit RNAPs, has been shown to rapidly oscillate (millisecond phase) between pre- and post-translocation positions.[20] Depending on the template position, the DNAP TEC can rest in a primarily pre-, post- or intermediate translocation position. The elongation complex only permits loading of dNTP substrates to the post-translocated DNAP, explaining the requirement for free pre-translocated to post-translocated (pre→post) DNAP sliding on template. Multi-subunit RNAPs, by contrast, do not necessarily make translocation excursions or load NTP substrates in similar modes or with similar rates to single subunit DNAPs.

Exonuclease (Exo) III has been used to infer the resting translocation register of RNAP TECs.[6,17,21-24] Here we use Exo III to probe the resting translocation states of various *E. coli* RNAP TECs to gain insight into translocation dynamics, the effects of TEC RNA length, the effects of nucleotide analogs, the effects of TGT and the effects of some RNAP mutants that restrain or stimulate the translocation ratchet. We conclude that *E. coli* RNAP makes the pre→post transition readily. Without NMP incorporation, the post-translocated TEC can advance by one or even two bases, which we refer to as hyper-translocated states.[25,26] The post→hyper transition is slow and is strongly inhibited by TGT. The post→pre transition is generally slow. The pre→backtracked transition is slow and is inhibited by TGT. From structures, bacterial RNAP TECs have a 9–10 nt RNA/DNA hybrid,[13,14] depending on whether the TEC is post- (9 nt) or pre-translocated (10 nt). Consistent with the 9–10 nt length of the RNA/DNA channel, a TEC with a 9 nt RNA strongly resists the post→pre transition and a TEC with a10 nt RNA makes the post→pre transition much more rapidly.

Results

***E. coli* RNAP rests post-translocated.** The data shown in **Figure 1** indicates that the *E. coli* RNAP TEC stalls primarily in a post-translocated register.[10] To describe the upstream border

*Correspondence to: Zachary F. Burton; Email: burton@cns.msu.edu
Submitted: 08/23/12; Revised: 09/19/12; Accepted: 09/20/12
http://dx.doi.org/10.4161/trans.22037

mapping experiment, we have readjusted our interpretation of Exo III bands in terms of the dominant relative position of the RNAP active site by one base upstream, compared with some recent reports.[21,23,24,27] Additional documentation in support of our re-evaluation is shown below. The downstream border Exo III mapping is described here as it was previously. One advantage to our re-evaluation of the DNA band pattern produced at the upstream TEC border is that it causes upstream and downstream border mapping to be consistent. A previous interpretation of the upstream RNAP boundaries would indicate, by contrast, that the G9 TEC is simultaneously primarily pre-translocated (mapped from upstream) and primarily post-translocated (mapped from downstream), which seems to require very rapid oscillation of RNAP and irresistible pushing of RNAP against Exo III. Below, we show that, at many positions, RNAP does not appear to rapidly progress post→pre and that Exo III appears to push on RNAP both from upstream and downstream borders. These observations indicate, therefore, that rapid RNAP oscillation may not be a correct interpretation of the upstream border Exo III mapping experiment. According to our reinterpretation, the G9 TEC is primarily post-translocated, mapped from either the upstream or the downstream RNAP border, and the pre→post transition is rapid, as required to support rapid RNAP elongation rates, so our band assignments appear to bring greater simplicity to the interpretation of the Exo III mapping experiment. Additionally, our interpretation indicates that the *E. coli* RNAP TEC can hyper-translocate.

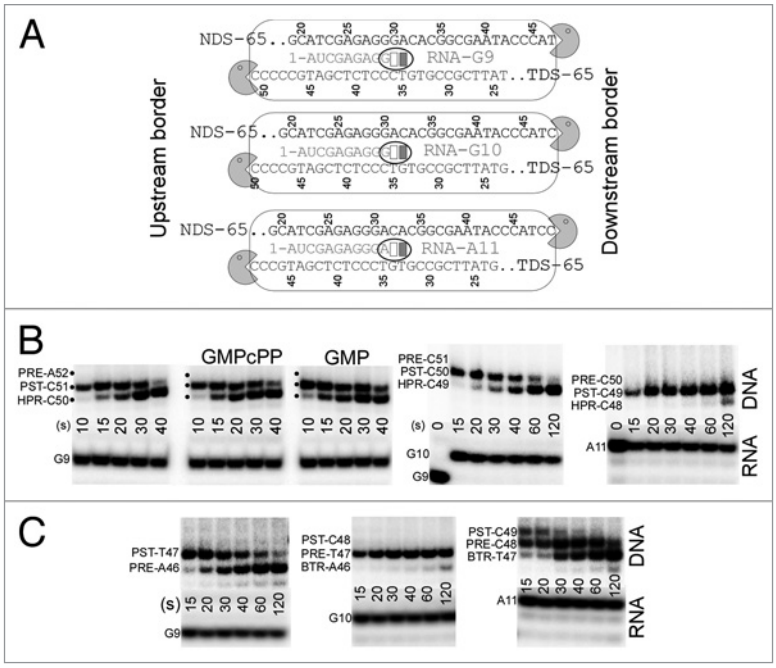

Figure 1. *E. coli* RNAP stalls in a primarily post-translocated register. (**A**) A schematic to describe the interpretation of the Exo III mapping experiment for G9, G10 and A11 TECs (large squared ovals), in terms of the correlation between upstream and downstream Exo III mapping bands for the post-translocated TEC and the RNAP active site. The pre-translocated boundary is one base upstream and the hyper-translocated boundary is one base downstream of the indicated boundaries. The three active site positions indicated (small ovals), are the pre- (RNA 3' end), post- (open rectangles) and hyper-translocated (gray rectangles) i+1 positions. (**B**) Upstream border Exo III mapping for G9, G10 and A11 TECs. GMPcPP and GMP (500 μM) were added to the G9 TEC as accurately templated non-incorporable GTP analogs. Exo III bands interpreted to arise from the backtracked (BTR), pre- (PRE), post- (PST) and hyper-translocated (HPR) TECs are indicated. (**C**) Downstream border Exo III mapping for G9, G10 and A11 TECs. RNA controls show that TECs do not overrun their intended stall positions. Five μM NTPs were added to advance TECs.

Figure 1A shows a schematic to describe the Exo III 3'→5' mapping experiment. To preserve the best possible record of translocation positions, a functionally saturating concentration of Exo III was used to attain rapid DNA digestion rates at 25°C. For these experiments, TECs are assembled with template strand DNA, RNA-G9 (a 9 nucleotide RNA ending in 3'GMP) and non-template strand DNA. Template and non-template DNAs are fully complementary over their 65 nucleotide lengths. Depending on the border to be mapped, the template or the non-template DNA strand was 5'labeled with ^{32}P. RNA-G9 was also 5'labeled to confirm that TEC RNAs were of the expected size. NTPs were added to form G10 or A11 TECs. The squared ovals indicate the extent on DNA of the post-translocated TEC, which we conclude is the dominant resting translocation state. To limit Exo III digestion to a single DNA strand, a thio-NMP was incorporated at the 3'end of the unlabeled DNA strand.[23]

Because Exo III encounters a TEC border that is located at a distance from the RNAP active site, to be informative, the pattern of DNA bands produced by Exo III digestion must be interpreted in terms of the active site translocation register. Despite a potential limitation that Exo III measures only single base increments as opposed to fractional translocation excursions, we find that the Exo III pattern can be interpreted and compared at many TEC positions. According to our evaluation, Exo III mapping from the upstream RNAP TEC border, the pre-translocated, post-translocated and hyper-translocated TECs generate DNA bands primarily 16, 15 and 14 nt upstream from the position of the RNA 3'end (counting the RNA 3'end as 1). These assignments represent a one nucleotide shift upstream compared with some previous interpretations.[21,23,24,27] Exo III mapping from the downstream border, the pre-translocated, post-translocated and hyper-translocated TECs generate DNA bands primarily 17, 18 and 19 nt downstream from the position of the RNA 3'end (counting from the next downstream position from the RNA 3'end). Some DNA bands could be stabilized by delayed Exo III digestion, approaching a RNAP border and/or oscillation between translocation states that is too rapid to expose a DNA site sufficiently for digestion.

In **Figure 1B**, the upstream TEC border is detected by Exo III. According to our interpretation, the pre-translocated register is essentially undetectable for G9, G10 and A11 TECs with 10 to 15 sec of Exo III digestion. If digestion is efficient, this result is reasonable because, to support elongation, translocation pre→post must occur with a rate of about 20–90 sec^{-1}. Mapping from the upstream border, Exo III detects the furthest excursions

of the TEC in the downstream direction. The pre-translocated TEC is not readily detected because it is converted to the post-translocated register, and the DNA template strand becomes shortened by Exo III within the 10–15 sec incubation. Of course, once Exo III digests the DNA, it remains shortened whether the TEC remains in a more downstream translocation register or returns upstream. Therefore, Exo III digestion rates from the upstream TEC border relate to downstream translocation rates but not to rates of RNAP returns upstream.

Exo III mapping from the upstream border indicates that the RNAP G9 TEC can hyper-translocate with longer periods of incubation. The Exo III DNA band that we interpret as representing the hyper-translocated G9 TEC (DNA-C50) is barely detectable with 10 or 15 sec of digestion. Previously, this band was interpreted as post-translocated,[23,24] but much stronger signals would be expected for the post-translocated G9 TEC after 10–15 sec of Exo III digestion. The A11 TEC is highly resistant to hyper-translocation, supporting our conclusion that the band that we interpret as hyper-translocated A11 (DNA-C48) cannot reasonably be interpreted as reflecting the post-translocated A11 TEC. RNAP TECs need not remain hyper-translocated to result in the shorter Exo III digestion length, because a brief excursion to the downstream position may be sufficient for DNA digestion by Exo III, and the DNA strand does not lengthen upon a return of RNAP upstream.

For the G9 TEC, we also test the addition of two non-incorporable GTP analogs, GMPcPP and GMP. Because G10 is the next position, GMPcPP and GMP are templated accurately at G10 and would be expected to strongly stimulate the pre→post translocation step for the pre-translocated G9 TEC. Significantly, however, in the Exo III experiment, neither GMPcPP nor GMP strongly stimulates apparent forward translocation of the resting G9 TEC, indicating that G9 is initially primarily post-translocated and therefore indifferent to nucleotides, rather than primarily pre-translocated and therefore sensitive to addition of nucleotides. This observation, therefore, strengthens the argument for our revised interpretations of Exo III digestion bands. The very weak GMPcPP and GMP effects for the G9 TEC seem inconsistent with the previous band assignments for upstream TEC border mapping.

A 9–10 nt RNA/DNA hybrid. Figure 1C shows downstream Exo III mapping of the G9, G10 and A11 TECs with our interpretation of Exo III DNA bands relative to the likely translocation register at the RNAP active site. Mapping the downstream border, we agree with the DNA band assignments made in previous publications.[21,27] The G9 TEC is slow to make the transition from post→pre, consistent with our band assignments, and, furthermore, as expected, the G9 TEC resists backtracking. The approximate $t_{1/2}$ for the post→pre transition for G9 is ~35 sec ($k = \sim 0.02\ sec^{-1}$). This value assumes that Exo III digestion is relatively efficient and generally cleaves the DNA at the next available position if the TEC becomes pre-translocated. G9 is a special case, because the RNA is barely long enough to fill the RNA/DNA hybrid channel of 10 nt in the post-translocated register.[13,14]

For the post→pre transition, the G10 TEC provides an interesting contrast to G9 and A11, indicative of a 9–10 nt RNA/DNA hybrid in bacterial RNAPs.[13,14] For the post→pre transition, G10 is much faster than G9 or A11. In this case the post→pre rate for G10 is too fast to measure within 15 sec, estimated at $k > 0.2\ sec^{-1}$ ($5*t_{1/2} < 15$ sec). For A11, the post→pre rate is slower than for G10 but faster than G9, estimated at $k = \sim 0.07\ sec^{-1}$ ($t_{1/2} = \sim 10$ sec). We posit that the G9 TEC prefers to rest in the post-translocated register, because this just fills the 10 nt RNA/DNA hybrid channel. The G10 TEC more easily resides in the pre-translocated register because when pre-translocated the G10 TEC just fills the 10 nt RNA/DNA channel. Because of its longer length, the A11 TEC appears to occupy the RNA exit channel more comfortably than G10. The post-translocated G10 TEC is expected to fit just one nucleotide into the RNA exit channel, which might enhance G10 upstream slippage. The post-translocated A11 TEC projects two nucleotides into the RNA exit channel, which appears to stabilize post-translocated A11 compared with post-translocated G10.

For TECs with short RNAs, the tendency to backtrack is also consistent with a 10 nt RNA/DNA hybrid channel for bacterial RNAPs. G9 and G10 TECs strongly resist backtracking by even one nucleotide. The A11 TEC backtracks by one nucleotide but not by two, consistent with the observations at G9 and G10. TECs with a 10 nt RNA in the RNA/DNA channel therefore appear to be favored over TECs with a 9 nt RNA in the channel. The rate of A11 backtracking is about $\sim 0.01\ sec^{-1}$ ($t_{1/2} = \sim 60$ sec). Once again, backtracking tendencies for G9, G10 and A11 TECs are very consistent with RNAP maintaining a 10 nt NTP and RNA/DNA hybrid channel, as indicated in RNAP TEC structures.

Note that, if the G9 TEC Exo III bands are properly assigned at the downstream RNAP border, by comparison, the G10 and A11 bands must also be properly assigned. The slow G9 and A11 post→pre rates compared with forward elongation rates indicate that, at many positions, *E. coli* RNAP resides primarily in the post-translocated state, making relatively rare excursions to the pre-translocated state. The G10 TEC is somewhat of an exception, probably because the pre-translocated G10 TEC just fills the 10 nt RNA/DNA hybrid channel. These rates also indicate that more rapid mapping of the upstream and downstream TEC borders may be useful to better understand the most central on-pathway translocation steps, which are the pre→post (upstream boundary) and the post→pre (downstream boundary) transitions. Because Exo III digestion appears somewhat slow and forward translocation must be at least as rapid as forward elongation, the pre→post transition may be too fast to measure using the Exo III mapping approach. The post→hyper transition is quite slow for G9 and G10 TECs ($k = \sim 0.02$ to $0.03\ sec^{-1}$; $t_{1/2} = \sim 20$–40 sec). For A11, the post→hyper transition is much slower. Note that, mapping from the upstream border, if the band we identify as hyper is designated instead as post, as it was previously assigned, impossibly slow rates are estimated for the pre→post A11 TEC transition (too slow to estimate on this time scale) compared with RNAP elongation rates ($k = \sim 20\ 90\ sec^{-1}$). Furthermore, this transition is not as sensitive to addition of NTP analogs as expected for the pre→post transition (**Fig. 1B**).

Upstream border mapping with Exo III added prior to NTPs. In **Figure 2**, in order to access the upstream RNAP border as quickly as possible, Exo III was added for 30 sec to G9 TECs before addition of NTPs. After Exo III had digested to the G9 TEC border, NTPs were added, and TECs were stalled at G10, A11 or C12. RNA-G10 and A11 TECs were obtained by adding GTP or GTP+ATP to G9 TECs (**Fig. 1A**). RNA-C12 was obtained by using a DNA template that encodes U13, so, in the absence of UTP, the TEC stalls at C12 with addition of GTP, ATP and CTP to G9 TECs (**Fig. 2C**). Faster time points were done using a Kintek RQF-3 rapid chemical quench flow instrument. The kinetics of Exo III band appearances, therefore, can be used to infer which DNA band is likely to correspond to the post- and hyper-translocated TECs at each stall position. Approaching the G10 stall, DNA-C50 appears to represent the G10 post-translocated TEC and DNA-C49 the hyper-translocated TEC (**Fig. 2A**). The $t_{1/2}$ for appearance of DNA-C49 is approximately 40 sec, indicating a rate of synthesis of k = ~0.02 sec^{-1}, which is much too slow for appearance of the G10 post-translocated TEC. By contrast, DNA-C50 appears prior to appearance of RNA-G10. The interpretation is that DNA-C50 initially represents TEC excursions to hyper-translocated G9, but, after GTP addition, DNA-C50 primarily represents post-translocated G10. This result shows that Exo III digestion is not much slower than RNAP elongation rates under these experimental conditions, making Exo III a reasonable probe of the resting TEC translocation state. Similarly to G10, stalling at A11, DNA-C49 appears at about the same time as A11 RNA is synthesized, as expected for the A11 post-translocated TEC (**Fig. 2B**). By strong contrast, DNA-C48 appears very slowly, consistent with the A11 hyper-translocated TEC. As also shown in **Figure 1B**, the A11 TEC very strongly resists hyper-translocation, indicating that the DNA-C48 band cannot represent the A11 post-translocated state. A11 is not a notable RNAP pausing site (**Fig. 2C**), so the A11 TEC must access the post-translocation state much faster than DNA-C48 appears from Exo III digestion (**Fig. 2B**). Stalling RNAP at C12, RNA-C12 appears just before DNA-C48, indicating that DNA-C48 relates to the post-translocated C12 TEC (**Fig. 2C**). After long periods of incubation (300 and 600 sec), DNA-C47 becomes prominent, indicating that DNA-C47 most likely relates to the hyper-translocated C12 TEC. Even at 2 sec after ATP, GTP and CTP addition, DNA-C47 was only weakly detected, which is inconsistent with DNA-C47 representing the post-translocated C12 TEC. The kinetics of Exo III DNA band appearance, therefore, strongly supports our assignments for the relationship between events at the RNAP active site and Exo III digestion at the TEC upstream border.

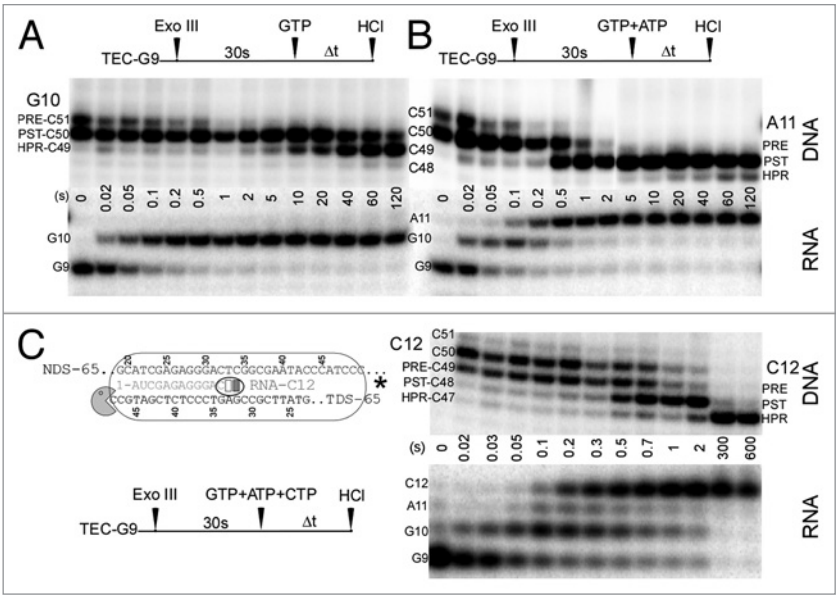

Figure 2. Upstream RNAP TEC border mapping with Exo III added prior to NTPs. (**A**) TEC stalled at G10 (see **Fig. 1A**); (**B**) TEC stalled at A11 (see **Fig. 1A**); and (**C**) TEC stalled at C12 (schematic), using a modified DNA template that encodes U13. Ten μM NTPs were added to advance TECs.

TGT suppresses hyper-translocation. The antibiotic TGT is hypothesized to stabilize the pre-translocated TEC by binding to the RNAP active site and mimicking pyrophosphate to restrain forward translocation.[10,17] TGT binding may also require a closed conformation of the trigger loop.[17] We therefore used TGT as a probe to help identify the pre-translocated register of the TEC as indicated by Exo III mapping at the upstream border. Mapping the upstream border in the presence of TGT was considered to be initially most important because we support a reinterpretation of the Exo III mapping data at the upstream but not at the downstream TEC border. Our experiment was designed for Exo III to digest rapidly to the upstream C14 TEC border in order to better detect the pre-translocation state, which might be short lived. To measure early time points, rapid chemical quench flow was used.

Using Exo III mapping at the upstream RNAP border, RNA-C14 TECs were analyzed for their resting translocation states in the absence and presence of TGT (**Fig. 3**). To improve detection of the pre-translocation state, a shortened ^{32}P-labeled TDS-50 was used so that only a short chain of CMP nucleotides needed to be digested for Exo III to reach the upstream C14 TEC border (**Fig. 3A**). Previous studies indicated that accurately paired poly-dC was a preferred Exo III substrate; therefore, digestion to the RNAP border was expected to be rapid.[23] **Figure 3B** shows gel data and **Figure 3C** shows representative quantification of the gel shown in **Figure 3B** and also an independent Exo III mapping experiment, with early time points done in triplicate. Comparing the 0.2 to 3 sec time points, TGT stabilizes detection of the pre-translocation state (DNA-C47) relative to the post-translocation state, as expected from the suggested mode of TGT RNAP inhibition (**Figs. 3B and 3C**). Comparing the 10, 20 and 30 sec time points, TGT strongly stabilizes detection of the Exo III band attributed to the post-translocation register (DNA-G46) and strongly suppresses appearance of the bands attributed to C14 hyper-translocation registers (DNA-T45

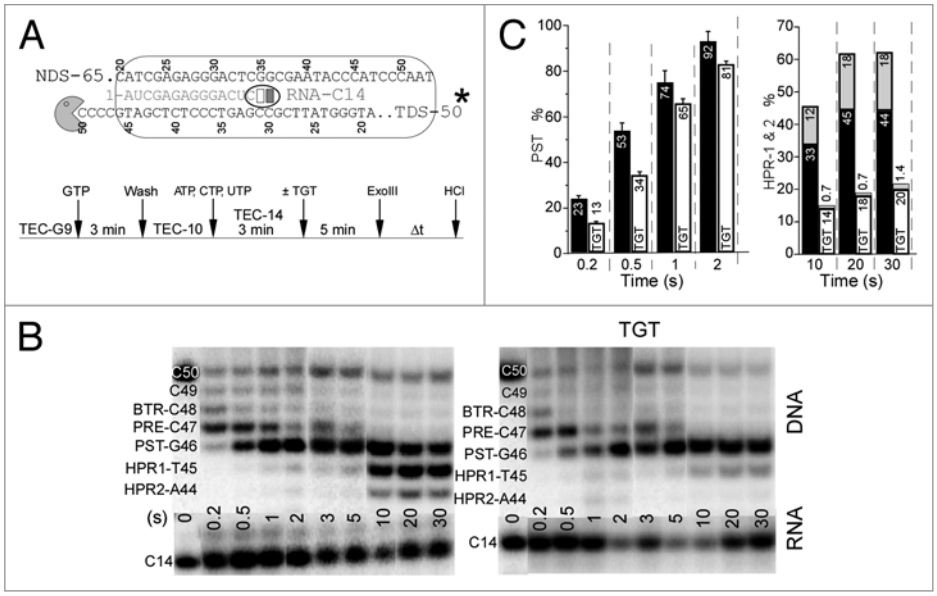

Figure 3. Tagetitoxin (TGT; 5 μM) stabilizes the pre- and post-translocation states and suppresses hyper-translocation. (**A**) C14 TECs were mapped at the upstream RNAP border with Exo III, as indicated in the schematic. (**B**) Gel data in the absence and presence of TGT. (**C**) Quantification of gels. (Left panel) A separate experiment done with triplicate points. Error bars indicate standard deviation. (Right panel) Quantification of data shown in **B**. Black bars represent DNA-T45 and gray bars represent DNA-A44. 100% is the sum of Exo III bands attributed to backtracked, pre-, post and hyper-translocated C14 TECs. 0.2 μM NTPs were added to advance TECs.

and A44). Because Exo III digestion from the upstream border gives a record of downstream excursions but not RNAP returns upstream, these observations could all be due to stabilization by TGT of the pre-translocated state of the RNAP TEC, as expected from a proposed mechanism of inhibition by TGT.[10,17] Because Exo III functions similarly to an integer ruler for translocation by cleaving DNA at phosphodiester bonds, TGT might stabilize a state that is fractionally forward translocated compared with the pre-translocation state detected by Exo III in the absence of TGT. Exo III only requires momentary exposure of a phosphodiester bond for digestion, so partial forward translocation in the presence of TGT, which might occur without opening of the trigger loop, might be indistinguishable using Exo III from full forward translocation in the absence of TGT. In this way, the DNA-G46 band could represent, primarily, a partially forward translocated TEC in the presence of TGT and a fully post-translocated TEC in the absence of TGT.

TGT suppresses RNAP backtracking. Because TGT affects Exo III mapping from the upstream RNAP TEC border (**Fig. 3**), the effects of TGT were also tested at the downstream border (**Fig. 4**). This experiment was designed to access the RNA-C14 TEC border rapidly, by shortening the 5'labeled non-template DNA strand on which Exo III acts to NDS-54 and by sampling rapid time points. For wild type RNAP, TGT slows the DNA-T53→A52 (hyper→post) and the A52→A51 (post→pre) transitions, but the main effect of TGT is to suppress backtracking (A51→shorter DNAs). For comparison to the wild type, bridge helix mutant β' F773V and a trigger loop deleted (Δ-TL) mutant RNAPs are shown. In other work, β' F773V has been shown to resist backtracking, so TGT has little effect on this mutant protein during the time course shown. The Δ-TL RNAP lacks some amino acid residues that are crucial for TGT binding, so, it is not surprising that this mutant shows no effects of TGT.[10,17,28] Furthermore, TGT competes with NTP substrates for RNAP binding, and the delta trigger loop mutant RNAP requires much higher NTP concentrations to advance to the C14 TEC position. To better understand the action of the TGT antibiotic, Exo III mapping is an informative approach.

Slow translocation ratchets. β' F773V and Δ-TL RNAPs have restrained translocation ratchets compared with wild type RNAP (**Figs. 4–6**). Comparing the DNA-T53→A52 (hyper→post) transition for wild type, β' F773V and Δ-TL RNAPs, the hyper→post transition is much faster for wild type RNAP than for β' F773V and Δ-TL RNAPs, indicating that wild type RNAP has a more active translocation ratchet and more rapid oscillation between translocation states than these two mutant proteins. The β' F773V substitution decreases bridge helix interactions with the extended β fork region explaining the effects of this substitution, because motions of the contacting β fork could facilitate movement of the β' bridge helix ratchet.[24,29] The trigger loop has previously been shown to be important for RNAP ratchet translocation.[27] In **Figure 5**, Exo III is used to map the RNA-G9 TEC from the downstream boundary. As was shown in **Figure 4** for the C14 TEC, for the G9 TEC, Δ-TL RNAP progresses more slowly than wild type RNAP post→pre (**Fig. 5**; compare 150 and 200 sec time points for wild type and Δ-TL RNAP). Comparing **Figures 4 and 5**, the C14 TEC has a more mobile translocation ratchet than the G9 TEC, which we attribute to the shorter G9 RNA length. These data show that Exo III mapping can be used to indicate the stiffness of the translocation ratchet at different TEC positions and also to discriminate RNAP mutant proteins from wild type and to begin characterization of likely mutant protein defects.

A hyperactive translocation ratchet. In **Figures 4 and 5**, we show that bridge helix β' F773V and Δ-TL mutant RNAPs have restrained translocation ratchets compared with wild type. In **Figure 6**, we show that a RNAP with a substitution in the bridge helix residue β' Y772A (adjacent to F773) has a hyperactive translocation ratchet in the absence of added substrate. Using Exo III mapping from the upstream RNAP border for G10 (**Fig. 6A**) and C14 TECs (**Fig. 6B**), β' Y772A RNAP makes the post→hyper transition more readily than wild type and β' F773V. As expected, β' F773V, with a restrained ratchet, is slowest in the post→hyper transition. Interestingly, the G10 TEC, which barely

fills the 10 nucleotide RNA/DNA channel in RNAP,[13,14] has a more restrained translocation ratchet than the C14 TEC. Once again, using Exo III mapping, relevant differences between RNAP mutant proteins and RNAP TECs with different short RNA lengths are revealed in translocation properties. Interestingly, addition of GMPcPP, a non-incorporable GTP analog, mostly suppresses differences between RNAP mutants and wild type, indicating that the translocation ratchet operates differently in the absence and presence of NTPs (**Figs. 6B and 6C**).

Hyper-translocation dependent on a templated NTP analog. Hyper-translocation by *E. coli* RNAP is apparently detected from both the upstream and downstream TEC borders, but the precise molecular meaning of these RNAP excursions is not completely clear, and Exo III mapping from opposite borders may provide somewhat different information. In **Figure 6B**, a two nucleotide step hyper-translocation is demonstrated mapping the upstream C14 TEC border in a reaction that is strongly dependent on a templated NTP analog. This result suggests that NTPs (perhaps two per template) can be loaded without incorporation, in upstream templated positions.

After 300 sec incubation with Exo III at the RNA-C14 TEC position, DNA-A44 (a two-step hyper-translocation product) is detected in a reaction that is very strongly dependent on addition of the GTP analog GMPcPP. At TEC-C14, GTP is accurately templated at the G15 and G16 positions, so there is a possibility of accurately loading one or two GMPcPP molecules on a single DNA template within a single TEC. The hyper-translocation reaction has not yet been completely analyzed for its DNA sequence specificity or its nucleotide dependence, but it is shown here as an added dimension of RNAP hyper-translocation and its potentially strong nucleotide dependence. Because such long incubation times are required, hyper-translocation by two nucleotide steps is not likely to be a frequent event for normal RNAP elongation; although, given high in vivo NTP concentrations, hyper-translocation could be a regulatory event at some template sequences; for instance, RNAP hyper-translocation may be associated with intrinsic termination.[25,26]

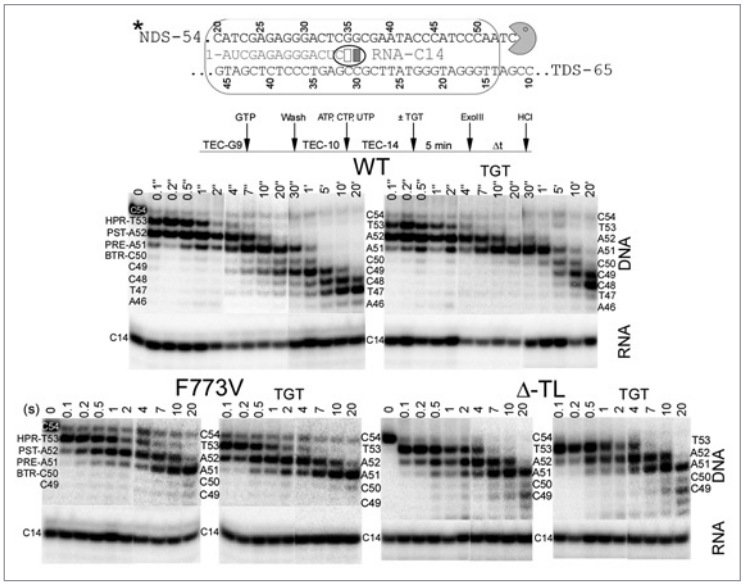

Figure 4. TGT (10 μM) stabilizes the pre-translocation state and suppresses backtracking. C14 TECs were mapped from the downstream boundary with Exo III (schematic). Wild type, β' F773V and Δ-TL RNAP in the absence and presence of TGT. 400 μM NTPs were added to advance the Δ-TL TEC. 0.2 μM NTPs were added to advance the wild type and β'F773V TECs.

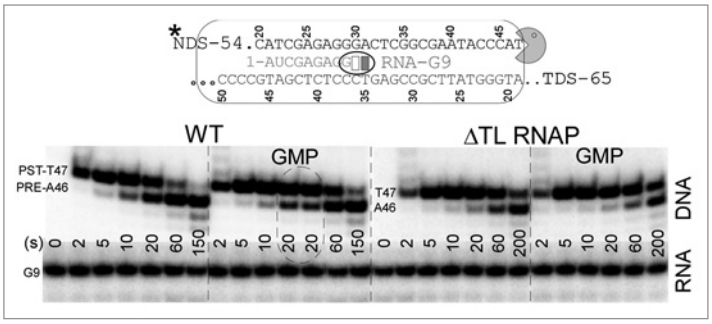

Figure 5. Δ-TL RNAP has a stiffer translocation ratchet than wild type RNAP. G9 TECs were mapped with Exo III from the downstream boundary. GMP (1 mM; accurately templated at G10) inhibits the G9 post→pre transition, as expected. The G9 TEC has a less active translocation ratchet compared with the C14 TEC (compare **Figs. 4 and 5**).

Exo III digestion to the RNAP TEC borders stimulates pyrophosphorolysis. Encounters of Exo III with an RNAP TEC border can be consequential. In **Figure 7**, we show the effects of Exo III digestion to the upstream or downstream boundary of the RNAP G9-TEC on pyrophosphorolysis.[21] We find that digestion to either border stimulates pyrophosphorolysis relative to a control including pyrophosphate but to which Exo III was not added. These data show that Exo III digestion to either RNAP border modifies the state of the resting TEC, as expected. With Exo III at the downstream border, Exo III might push the TEC in the upstream direction to stimulate pyrophosphorolysis. Alternatively, increasing the flexibility of downstream DNA by rendering the template DNA single-stranded could stimulate the TEC to slip backward; although, in this case, the mechanism for increasing slippage is less apparent. It is likely that upstream Exo III mapping facilitates RNAP slipping backward by rendering the non-template DNA single-stranded. These experiments indicate that Exo III digestion to the RNAP boundaries perturbs some features of TECs. It is not clear that these perturbations undermine the utility of the Exo III digestion experiment, but they should be considered in interpretation of mapping results. Significantly, we show here that post→pre transitions for *E. coli* RNAP TECs are surprisingly slow (**Fig. 1**); although, based on the results in **Figure 7**, these very slow rates appear to be stimulated by Exo III contacting the downstream RNAP boundary. In the absence of Exo III, post→pre rates might be slower.

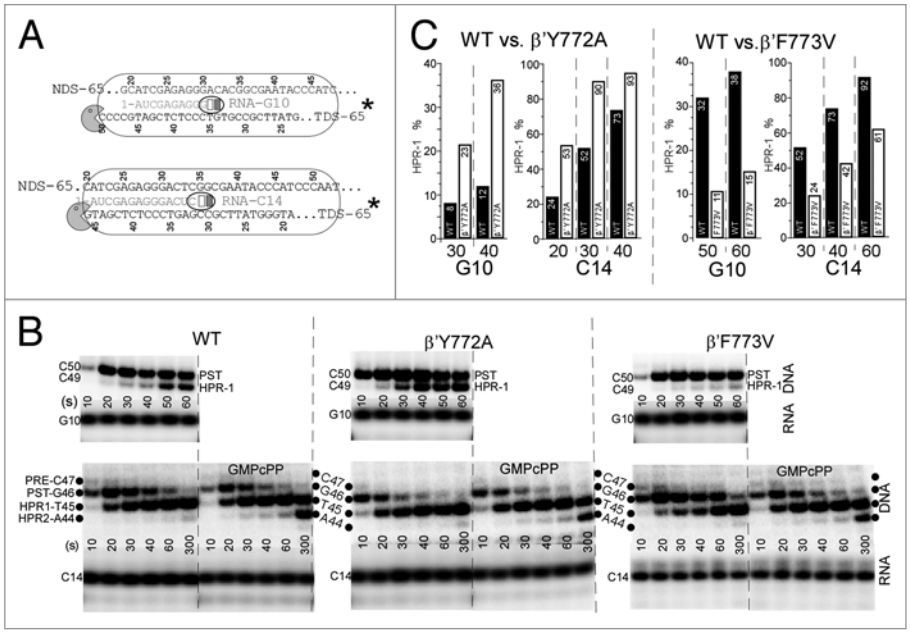

Figure 6. TEC G10 has a less active translocation ratchet compared with TEC C14. β' Y772A has a more active translocation ratchet than wild type RNAP. β' F773V has a stiffer translocation ratchet than wild type RNAP. RNAP hyper-translocation by two nucleotide steps is strongly dependent on a templated GTP analog (GMPcPP; 500 μM). Hyper-translocation by two nucleotide steps is demonstrated for wild type and two bridge helix mutant RNAPs (β' Y772A and F773V). (**A**) Exo III mapping was from the upstream G10 and C14 TEC borders as indicated in the schematics. (**B**) Exo III mapping gels with RNA controls. (**C**) Quantification of representative gel data from B. 0.2 μM NTPs were added to advance TECs.

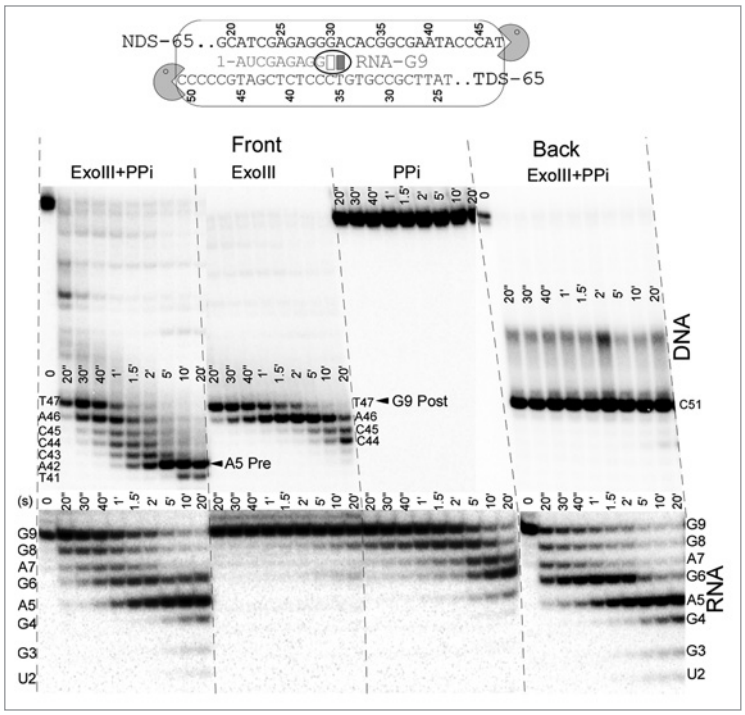

Figure 7. Exo III digestion to the upstream or the downstream G9 TEC border stimulates pyrophosphorolysis. Four mM pyrophosphate (PPi) was added to reactions, as indicated.

Discussion

Exo III mapping has been used to analyze translocation of resting *E. coli* RNAP TECs. Stalling of TECs appears to be primarily in the post-translocated register,[10] and TECs also have a tendency to hyper-translocate. Hyper-translocation is apparently detected with Exo III mapping from both the upstream and downstream RNAP borders, indicating that this may be a significant feature of RNAP stalling. It was previously suggested that hyper-translocation by *E. coli* RNAP is a feature of intrinsic termination mechanisms, which involve formation of a RNA stem loop structure followed by a U-stretch.[25,26,30-32] The intrinsic termination mechanism may include: (1) formation of the RNA stem-loop and RNAP pausing; (2) possible invasion of the DNA template channel by the RNA stem and; (3) leveraged dissociation of the U-stretch from its poly-dA template. We show here that the antibiotic TGT strongly inhibits hyper-translocation raising the question of whether TGT might inhibit intrinsic termination by blocking RNAP hyper-translocation. In other work, we demonstrate that the bridge helix β' F773V substitution, which we show here resists hyper-translocation (**Fig. 6**), is also defective in bacteriophage λ tR2 intrinsic termination, consistent with hyper-translocation contributing to intrinsic termination.

The extent to which RNAP TECs freely oscillate between pre- and post-translocation states has not been determined. From Exo III mapping, it appears that the pre→post transition may be much more rapid than the post→pre transition at many TEC positions, indicating that RNAP may rest primarily post-translocated without frequent pre↔post oscillation.[10] As judged from Exo III mapping, at many TEC positions, RNAP appears to oscillate in a post→hyper mode almost as frequently as in a post→pre mode. A direct, single-TEC approach[20] to measure RNAP transitions will be necessary to fully resolve the issue of resting RNAP oscillation. Significantly, however, rapid TEC oscillation pre↔post is not necessary to explain Exo III mapping results or fluorescence analysis of TEC translocation[10] and appears inconsistent with both types of experiment. Molecular dynamics simulations do not reveal significant RNAP TEC sliding or pre↔post oscillation and appear most consistent with a model in which bending at the bridge helix β' 778-GARKGL-783 glycine hinge against the RNA/DNA hybrid induces phosphodiester bond completion and forward translocation.[24,29]

TECs containing short RNAs of 9, 10 and 11 nt have translocation properties that are highly consistent with a

9–10 bp RNA/DNA hybrid, as observed in crystal structures.[13,14] As an example, the G9 TEC appears to be primarily post-translocated whether mapped from the upstream or the downstream RNAP boundary. For G9, the pre→post transition appears to be rapid, and the post→pre transition appears to be very slow (k = ~0.02 sec^{-1}; $t_{1/2}$ = ~20–30 sec). A 10 nt NTP and RNA/DNA hybrid channel[13,14] is just filled by the G9 TEC in a post-translocated register, potentially stabilizing G9 in the post-translocated state relative to the pre-translocated state (**Fig. 1**). Consistent with this idea, compared with G10 and A11 TECs, the G9 TEC strongly resists the post→pre transition. Because G9 resists entering the pre-translocated state, G9 also strongly resists backtracking, which requires an additional step upstream and limits the length of the RNA/DNA hybrid to 8 nt. When Exo III is at the G9 TEC upstream border, hyper-translocation is evident, perhaps in part because of collision of Exo III with RNAP, inducing forward displacement. The G10 TEC also resists backtracking, but the A11 TEC backtracks (k = ~0.01 sec^{-1}; $t_{1/2}$ = ~60 sec) by one nucleotide but not readily by two. Interestingly, G10 has a faster post→pre transition than G9 or A11, probably because, at 10 nucleotides, the RNA has just begun to dissociate from the 10 nt RNA/DNA hybrid channel in the post-translocation state, but, in the pre-translocation state, G10 just fills the 10 nt RNA/DNA hybrid channel. We posit, therefore, that the 10 nt RNA length stabilizes the pre-translocated G10 TEC relative to the post-translocated G10 TEC. Compared with G9 and G10, the A11 TEC strongly resists hyper-translocation. Exo III mapping, therefore, discriminates between different TECs and their individual characteristics. Short RNA lengths of 9 to 11 nucleotides have profound and distinct characteristics for translocation mostly based on their ability to fit the 10 nucleotide RNA/DNA channel and their ability to stably enter the RNA exit channel.

Exo III mapping also gives insight into mutant proteins and their differences from wild type RNAP. β' F773V and Δ-TL RNAPs appear to have stiffer translocation ratchets compared with wild type RNAP. These mutants resist backtracking and show resistance to TGT, which also inhibits backtracking by stabilizing the pre-translocated TEC. β' F773 projects from the bridge helix into the β fork, so a F773V substitution might be less influenced by fork contacts, decreasing bridge helix bending in response to motions of the fork. Deletion of the trigger loop uncouples loop closing from bridge helix bending, decreasing the activity of the translocation ratchet, as observed by Exo III mapping (**Figs. 4 and 5**). The bridge helix mutant β' Y772A, by contrast, has a hyperactive bridge helix ratchet (**Fig. 6**). The β' Y772A substitution removes a hydrogen bond to the β link domain D674 main chain oxygen.[13,14] In wild type, the Y772-D674 hydrogen bond connection couples the bridge helix N-terminal segment to the active site, and breaking this connection by the alanine substitution appears to relieve this restraint, resulting in greater bridge helix bending and a more active translocation ratchet. Based on molecular dynamics simulations and biochemical approaches, we posit that the RNAP translocation ratchet involves bending primarily at the bridge helix β' 778-GARKGL-783 glycine hinge as influenced by surrounding protein including the β fork and the β' trigger loop.[24,29,33,34] Decreasing fork-bridge contacts (β' F773V) or trigger loop-bridge helix contacts (Δ-TL) would be expected to stiffen the translocation ratchet by deleveraging bridge helix bending at the hinge. By contrast, weakening the connection between the bridge helix, the link domain and the active site in β' Y772A appears to break a feedback circuit in which a NTP substrate in the active site restrains the bridge helix glycine hinge to favor catalysis rather than translocation. We posit, therefore, that the Y772A substitution might be expected to allow increased and unregulated flexibility of the bridge helix glycine hinge by breaking the Y772-D674 connection. These regulatory circuits are described in more detail in work submitted for publication.

Recent models for TGT inhibition of *E. coli* RNAP indicate that TGT binds to a pre-translocated RNAP TEC with a closed conformation of the trigger loop, which is expected to block the pre→post transition.[10,17] Based on these models and fluorescence studies of RNAP translocation, therefore, we expected TGT to block the pre→post and the pre→backtracked transitions by stabilization of the pre-translocation register. Using Exo III to analyze TGT effects, however, appears to produce a slightly unexpected result. With Exo III, TGT weakly inhibits the pre→post transition, as expected, but much more strongly appears to inhibit the post→hyper transition (**Fig. 3**). As expected, using Exo III, TGT strongly inhibits the pre→backtracked transition. Therefore, using either Exo III mapping or fluorescence detection, TGT blocks backward and forward translocation from the pre-translocation register, but, using Exo III, TGT does not appear to block the pre→post transition as strongly as would be expected from the fluorescence data.[10] This apparent difference between Exo III and fluorescence measurements may be due to the ability of Exo III at the upstream RNAP TEC border to detect a fractional forward translocation shift by exposure of a phosphodiester bond on the DNA template strand. If this explanation and recent models for TGT action are correct, Exo III experiments indicate that significant forward translocation may occur prior to opening of the trigger loop, as if bridge helix bending against the RNA/DNA hybrid continues to tighten the active site after phosphodiester bond formation, as part of a bond completion mechanism.[24]

Exo III and fluorescence are complimentary approaches to analyze RNAP translocation. Because Exo III cleaves DNA 3'→5' in single base steps, Exo III reveals translocation registers similarly to an integer ruler, potentially neglecting or alternatively strongly reflecting fractional RNAP movements depending on whether the next DNA cleavage site remains hidden or becomes exposed. Fluorescence changes, by contrast, are most sensitive to changes in the local probe environment, so a fluorescence signal can potentially saturate and, therefore, may not continue to increase with continued downstream RNAP translocation. The fluorescence probe utilized in the *E. coli* RNAP study was designed to be most sensitive to fractional RNAP movements close to the pre-translocated register[10] and may therefore be less responsive to RNAP movements further downstream, such as hyper-translocation. The fluorescence measurement, therefore, may not readily discriminate fractional post- from fully post- or from hyper-translocation positions if continued downstream translocation maintains the optical probe in a similar environment. This may explain some apparent differences we observe

comparing fluorescence experiments and Exo III mapping. The Exo III reaction measures exposure of DNA cleavage sites, without reporting the precise fractional translocation register, which must be inferred. Because TGT inhibits backtracking (**Fig. 4**), TGT stabilizes the pre-translocated TEC, as expected from models of TGT action.[10,17] According to Exo III mapping, TGT also appears to stabilize a post-translocated TEC to block hypertranslocation, although from fluorescence measurements, TGT appeared to specifically suppress the pre→post transition.[10] Exo III mapping and fluorescence approaches, therefore, provide slightly different insight into RNAP translocation. Both methods support a primarily post-translocated resting RNAP TEC. TGT is shown by both methods to block forward translocation, although from Exo III mapping it appears that the post→hyper transition may be more strongly inhibited, and from fluorescence it appears that the pre→post transition is most strongly blocked,[10] indicating that Exo III detects fractional forward movement of the TEC that was not strongly detected using fluorescent translocation probes.

As expected, Exo III encounters with the RNAP upstream and downstream TEC borders can be consequential. We show that Exo III digesting DNA to the upstream RNAP border stimulates pyrophosphorolysis compared with a TEC on a fully double-stranded DNA (**Fig. 7**). We attribute this stimulation to RNAP slipping backward more readily on a single-stranded nontemplate DNA strand to enhance pyrophosphorolysis. With Exo III at the downstream TEC border, pyrophosphorolysis is also stimulated but probably by a different mechanism. In this case, it appears that Exo III colliding with the downstream TEC border may stimulate RNAP slippage upstream. Remarkably, as estimated from Exo III mapping, the post→pre transition appears to be very slow under conditions in which Exo III at the downstream RNAP TEC border is expected to accelerate the post→pre transition, because Exo III at the downstream border stimulates pyrophosphorolysis, indicating stimulation of upstream RNAP movement.

Materials and Methods

Constructs. The trigger loop deleted (Δ-TL) RNAP has the following sequence compared with wild type RNAP: PGT QLT MRT FHI GGA DIT GGL PRV A (wild type→ PGTQ..... ..G.....GGLPRVA(Δ-TL) (from V. Svetlov). Other constructs are described in another manuscript submitted for publication.

Exonuclease III footprinting. Exo III mapping of *E. coli* RNAP TECs assembled in vitro was done as previously described.[23,24] RNAPs had a poly-histidine tag to facilitate immobilization and walking.[35-37] Exo III mapping was done on TECs released from beads with imidazole. G9 TECs were advanced to various positions, as indicated in the figures and described in the text. G9 RNA (AUCGAGAGG) was 5'-^{32}P-labeled. Depending on whether mapping was from upstream or downstream, the DNA template strand (upstream border mapping) or DNA non-template strand (downstream border mapping) was 5'-^{32}P-labeled for detection on gels. The cDNA strand was blocked for Exo III digestion by incorporation of a 3'-thio NMP. *E. coli* Exo III (New England Biolabs) mapping (4 units/μl) was at 25°C. Four units/μl Exo III is found to be functionally saturating to enhance Exo III digestion rates and to preserve a reliable record of RNAP translocation registers. The reaction buffer was 20 mM TRIS-HCl pH 7.9, 40 mM KCl, 5 mM $MgCl_2$, 5% glycerol, 0.003% IGEPAL CA-630 (Sigma), 10 μM $ZnS0_4$ and 1 mM β-mercaptoethanol. To some reactions, GMPcPP (α-β-methylene GTP) or GMP was added as a non-incorporable GTP analog. The antibiotic TGT[28,38,39] was added, as indicated. RNAs and DNAs were analyzed on 20% or 6% polyacrylamide-7M urea gels and quantified using a phosphorimager (Amersham Biosciences; Typhoon 9200).

Disclosure of Potential Conflict of Interest

No potential conflicts of interest were disclosed.

Acknowledgments

This work was supported by the National Science Foundation MCB-1050867 (70%) [to Z.F.B. (PI) and Robert I. Cukier (co-I)] and the National Institutes of Health R01 GM 092949 (30%) to Michael Feig (PI) and Z.F.B. (co-I). This work was supported by National Institutes of Health grant R01 GM58750 to E.N. Z.F.B. receives support from Michigan State University, the Michigan State University Agricultural Experiment Station, and the Michigan State University College of Osteopathic Medicine.

References

1. Kennedy SR, Erie DA. Templated nucleoside triphosphate binding to a noncatalytic site on RNA polymerase regulates transcription. Proc Natl Acad Sci U S A 2011; 108:6079-84; PMID:21447716; http://dx.doi.org/10.1073/pnas.1011274108.
2. Erie DA, Kennedy SR. Forks, pincers, and triggers: the tools for nucleotide incorporation and translocation in multi-subunit RNA polymerases. Curr Opin Struct Biol 2009; 19:708-14; PMID:19913407; http://dx.doi.org/10.1016/j.sbi.2009.10.008.
3. Foster JE, Holmes SF, Erie DA. Allosteric binding of nucleoside triphosphates to RNA polymerase regulates transcription elongation. Cell 2001; 106:243-52; PMID:11511351; http://dx.doi.org/10.1016/S0092-8674(01)00420-2.
4. Holmes SF, Erie DA. Downstream DNA sequence effects on transcription elongation. Allosteric binding of nucleoside triphosphates facilitates translocation via a ratchet motion. J Biol Chem 2003; 278:35597-608; PMID:12813036; http://dx.doi.org/10.1074/jbc.M304496200.
5. Kireeva M, Kashlev M, Burton ZF. Translocation by multi-subunit RNA polymerases. Biochim Biophys Acta 2010; 1799:389-401; PMID:20097318; http://dx.doi.org/10.1016/j.bbagrm.2010.01.007.
6. Bar-Nahum G, Epshtein V, Ruckenstein AE, Rafikov R, Mustaev A, Nudler E. A ratchet mechanism of transcription elongation and its control. Cell 2005; 120:183-93; PMID:15680325; http://dx.doi.org/10.1016/j.cell.2004.11.045.
7. Nudler E. RNA polymerase active center: the molecular engine of transcription. Annu Rev Biochem 2009; 78:335-61; PMID:19489723; http://dx.doi.org/10.1146/annurev.biochem.76.052705.164655.
8. Larson MH, Zhou J, Kaplan CD, Palangat M, Kornberg RD, Landick R, et al. Trigger loop dynamics mediate the balance between the transcriptional fidelity and speed of RNA polymerase II. Proc Natl Acad Sci U S A 2012; 109:6555-60; PMID:22493230; http://dx.doi.org/10.1073/pnas.1200939109.
9. Zhang J, Palangat M, Landick R. Role of the RNA polymerase trigger loop in catalysis and pausing. Nat Struct Mol Biol 2010; 17:99-104; PMID:19966797; http://dx.doi.org/10.1038/nsmb.1732.
10. Malinen AM, Turtola M, Parthiban M, Vainonen L, Johnson MS, Belogurov GA. Active site opening and closure control translocation of multisubunit RNA polymerase. Nucleic Acids Res 2012; 40:7442-51; PMID:22570421; http://dx.doi.org/10.1093/nar/gks383.

11. Brueckner F, Armache KJ, Cheung A, Damsma GE, Kettenberger H, Lehmann E, et al. Structure-function studies of the RNA polymerase II elongation complex. Acta Crystallogr D Biol Crystallogr 2009; 65:112-20; PMID:19171965; http://dx.doi.org/10.1107/S0907444908039875.
12. Brueckner F, Cramer P. Structural basis of transcription inhibition by alpha-amanitin and implications for RNA polymerase II translocation. Nat Struct Mol Biol 2008; 15:811-8; PMID:18552824; http://dx.doi.org/10.1038/nsmb.1458.
13. Vassylyev DG, Vassylyeva MN, Perederina A, Tahirov TH, Artsimovitch I. Structural basis for transcription elongation by bacterial RNA polymerase. Nature 2007; 448:157-62; PMID:17581590; http://dx.doi.org/10.1038/nature05932.
14. Vassylyev DG, Vassylyeva MN, Zhang J, Palangat M, Artsimovitch I, Landick R. Structural basis for substrate loading in bacterial RNA polymerase. Nature 2007; 448:163-8; PMID:17581591; http://dx.doi.org/10.1038/nature05931.
15. Wang D, Bushnell DA, Westover KD, Kaplan CD, Kornberg RD. Structural basis of transcription: role of the trigger loop in substrate specificity and catalysis. Cell 2006; 127:941-54; PMID:17129781; http://dx.doi.org/10.1016/j.cell.2006.11.023.
16. Kettenberger H, Armache KJ, Cramer P. Complete RNA polymerase II elongation complex structure and its interactions with NTP and TFIIS. Mol Cell 2004; 16:955-65; PMID:15610738; http://dx.doi.org/10.1016/j.molcel.2004.11.040.
17. Artsimovitch I, Svetlov V, Nemetski SM, Epshtein V, Cardozo T, Nudler E. Tagetitoxin inhibits RNA polymerase through trapping of the trigger loop. J Biol Chem 2011; 286:40395-400; PMID:21976682; http://dx.doi.org/10.1074/jbc.M111.300889.
18. Klyuyev S, Vassylyev DG. The binding site and mechanism of the RNA polymerase inhibitor tagetitoxin: an issue open to debate. Transcription 2012; 3:46-50; PMID:22414754; http://dx.doi.org/10.4161/trns.19468.
19. Svetlov V, Artsimovitch I, Nudler E. Response to Klyuyev and Vassylyev: on the mechanism of tagetitoxin inhibition of transcription. Transcription 2012; 3:51-5; PMID:22414748; http://dx.doi.org/10.4161/trns.19749.
20. Dahl JM, Mai AH, Cherf GM, Jetha NN, Garalde DR, Marziali A, et al. Direct observation of translocation in individual DNA polymerase complexes. J Biol Chem 2012; 287:13407-21; PMID:22378784; http://dx.doi.org/10.1074/jbc.M111.338418.
21. Hein PP, Palangat M, Landick R. RNA transcript 3'-proximal sequence affects translocation bias of RNA polymerase. Biochemistry 2011; 50:7002-14; PMID:21739957; http://dx.doi.org/10.1021/bi200437q.
22. Kireeva ML, Kashlev M. Mechanism of sequence-specific pausing of bacterial RNA polymerase. Proc Natl Acad Sci U S A 2009; 106:8900-5; PMID:19416863; http://dx.doi.org/10.1073/pnas.0900407106.
23. Kireeva ML, Nedialkov YA, Cremona GH, Purtov YA, Lubkowska L, Malagon F, et al. Transient reversal of RNA polymerase II active site closing controls fidelity of transcription elongation. Mol Cell 2008; 30:557-66; PMID:18538654; http://dx.doi.org/10.1016/j.molcel.2008.04.017.
24. Kireeva ML, Opron K, Seibold SA, Domecq C, Cukier RI, Coulombe B, et al. Molecular dynamics and mutational analysis of the catalytic and translocation cycle of RNA polymerase. BMC Biophys 2012; 5:11; PMID:22676913; http://dx.doi.org/10.1186/2046-1682-5-11.
25. Larson MH, Greenleaf WJ, Landick R, Block SM. Applied force reveals mechanistic and energetic details of transcription termination. Cell 2008; 132:971-82; PMID:18358810; http://dx.doi.org/10.1016/j.cell.2008.01.027.
26. Santangelo TJ, Roberts JW. Forward translocation is the natural pathway of RNA release at an intrinsic terminator. Mol Cell 2004; 14:117-26; PMID:15068808; http://dx.doi.org/10.1016/S1097-2765(04)00154-6.
27. Toulokhonov I, Zhang J, Palangat M, Landick R. A central role of the RNA polymerase trigger loop in active-site rearrangement during transcriptional pausing. Mol Cell 2007; 27:406-19; PMID:17679091; http://dx.doi.org/10.1016/j.molcel.2007.06.008.
28. Vassylyev DG, Svetlov V, Vassylyeva MN, Perederina A, Igarashi N, Matsugaki N, et al. Structural basis for transcription inhibition by tagetitoxin. Nat Struct Mol Biol 2005; 12:1086-93; PMID:16273103; http://dx.doi.org/10.1038/nsmb1015.
29. Weinzierl RO. The nucleotide addition cycle of RNA polymerase is controlled by two molecular hinges in the Bridge Helix domain. BMC Biol 2010; 8:134; PMID:21034443; http://dx.doi.org/10.1186/1741-7007-8-134.
30. Gusarov I, Nudler E. The mechanism of intrinsic transcription termination. Mol Cell 1999; 3:495-504; PMID:10230402; http://dx.doi.org/10.1016/S1097-2765(00)80477-3.
31. Nudler E, Gusarov I. Analysis of the intrinsic transcription termination mechanism and its control. Methods Enzymol 2003; 371:369-82; PMID:14712715; http://dx.doi.org/10.1016/S0076-6879(03)71028-3.
32. Toulokhonov I, Landick R. The flap domain is required for pause RNA hairpin inhibition of catalysis by RNA polymerase and can modulate intrinsic termination. Mol Cell 2003; 12:1125-36; PMID:14636572; http://dx.doi.org/10.1016/S1097-2765(03)00439-8.
33. Seibold SA, Singh BN, Zhang C, Kireeva M, Domecq C, Bouchard A, et al. Conformational coupling, bridge helix dynamics and active site dehydration in catalysis by RNA polymerase. Biochim Biophys Acta 2010; 1799:575-87; PMID:20478425; http://dx.doi.org/10.1016/j.bbagrm.2010.05.002.
34. Weinzierl RO. The Bridge Helix of RNA polymerase acts as a central nanomechanical switchboard for coordinating catalysis and substrate movement. Archaea 2011; 2011:608385; PMID:22312317; http://dx.doi.org/10.1155/2011/608385.
35. Nudler E, Gusarov I, Bar-Nahum G. Methods of walking with the RNA polymerase. Methods Enzymol 2003; 371:160-9; PMID:14712698; http://dx.doi.org/10.1016/S0076-6879(03)71011-8.
36. Kashlev M, Martin E, Polyakov A, Severinov K, Nikiforov V, Goldfarb A. Histidine-tagged RNA polymerase: dissection of the transcription cycle using immobilized enzyme. Gene 1993; 130:9-14; PMID:8344532; http://dx.doi.org/10.1016/0378-1119(93)90340-9.
37. Kashlev M, Nudler E, Severinov K, Borukhov S, Komissarova N, Goldfarb A. Histidine-tagged RNA polymerase of Escherichia coli and transcription in solid phase. Methods Enzymol 1996; 274:326-34; PMID:8902816; http://dx.doi.org/10.1016/S0076-6879(96)74028-4.
38. Steinberg TH, Burgess RR. Tagetitoxin inhibition of RNA polymerase III transcription results from enhanced pausing at discrete sites and is template-dependent. J Biol Chem 1992; 267:20204-11; PMID:1400338.
39. Steinberg TH, Mathews DE, Durbin RD, Burgess RR. Tagetitoxin: a new inhibitor of eukaryotic transcription by RNA polymerase III. J Biol Chem 1990; 265:499-505; PMID:2403565.